Origin of Enhanced Stem Cell Growth and Differentiation on Graphene and Graphene Oxide

Wong Cheng Lee,[†,§,∥] Candy Haley Y. X. Lim,[†,‡,∥] Hui Shi,[⊥] Lena A. L. Tang,[‡] Yu Wang,[‡] Chwee Teck Lim,[†,§,⊥,*] and Kian Ping Loh[‡,*]

[†]NUS Graduate School for Integrative Sciences and Engineering, Centre for Life Sciences #05-01, National University of Singapore, 28 Medical Drive, 117456, Singapore, [‡]Department of Chemistry, National University of Singapore, Science Drive 3, 117543, Singapore, [§]Division of Bioengineering and Department of Mechanical Engineering, National University of Singapore, 7 Engineering Drive 1, 117574, Singapore, and [⊥]Mechanobiology Institute, National University of Singapore, T-Lab, #05-01, 5A Engineering Drive 1, 117411, Singapore. [∥]These authors contributed equally.

ABSTRACT The culture of bone marrow derived mesenchymal stem cells (MSCs), as well as the control of its differentiation toward different tissue lineage, is a very important part of tissue engineering, where cells are combined with artificial scaffold to regenerate tissues. Graphene (G) and graphene oxide (GO) sheets are soft membranes with high in-plane stiffness and can potentially serve as a biocompatible, transferable, and implantable platform for stem cell culture. While the healthy proliferation of stem cells on various carbon platforms has been demonstrated, the chemical role of G and GO, if any, in guiding uncommitted stem cells toward differentiated cells is not known. Herein, we report that the strong noncovalent binding abilities of G allow it to act as a preconcentration platform for osteogenic inducers, which accelerate MSCs growing on it toward the osteogenic lineage. The molecular origin of accelerated differentation is investigated by studying the binding abilities of G and GO toward different growth agents. Interestingly, differentiation to adipocytes is greatly suppressed on G because insulin, which is a key regulator for the synthesis of fatty acids, is denatured upon $\pi-\pi$ adsorption on G; in contrast, GO does not interfere with adipogenesis due to electrostatic binding with insulin. The different binding interactions and their subsequent influence on stem cell growth and differentiation are ascribed to different degrees of $\pi-\pi$ stacking and electrostatic and hydrogen bonding mediated by G and GO.

KEYWORDS: graphene · graphene oxide · stem cells · differentiation · preconcentration

Mesenchymal stem cells (MSCs) isolated from adult bone marrow are multipotent progenitor cells noted for their potential to differentiate into cell lineages such as adipocytes, osteoblasts, and chondrocytes.[1] By manipulating material mechanics,[2] substrate topography,[3] and applied growth factor inducers,[4] MSCs can be induced to differentiate into desired cell types applicable in tissue engineering and regenerative medicine. Many biochemists and molecular biologists employ chemical factors to induce differentiation *in vitro*, but guided differentiation of stem cells using these strategies is not efficient and often requires weeks to months of cell culture for maturation into distinct lineages.[5] This has limited the widespread use of stem cell therapy. Therefore, there is a need to develop efficient methods for enhancing MSC differentiation.

There is a drive to search for biocompatible and mechanically stable platforms for *in vivo* implant technology for delivering stem cells.[6,7] Certain nanomaterials were found to be able to enhance stem cell proliferation and lineage specification, although the chemical origins of these can be complex.[8−11] Aqueous suspensions of carbon nanotubes[12] and gold nanoparticles[13] have been demonstrated to enhance osteogenesis. A stress mechanism was suggested to be operational, brought about by the interaction of these nanomaterials with the cell membrane as well as binding with proteins in the cytoplasm, which activated the p38 mitogen-activated protein kinase (MAPK) signaling pathway responsible for regulating the expression of genes inducing osteogenic transcription.[13] Glass substrates coated with bionanoparticles such as turnip yellow mosaic (TYMV) and tobacco mosaic virus (TMV) have also been shown to stimulate MSC osteogenic differentiation and bone matrix mineralization, and factors such as the nanoscale topography, serum protein adsorption by viruses, or interaction with certain cellular receptors have been proposed.

Atomically thin graphene (G) and graphene oxides (GO) sheets are biocompatible platforms that have the potential to mediate stem cell lineage specification for tissue regeneration. G is characterized by a purely carbon, aromatic network that presents an open surface for noncovalent interaction with biomolecules. G can now be produced in large areas by chemical vapor deposition (CVD) on copper foil.[16] GO can

* Address correspondence to ctlim@nus.edu.sg, chmlohkp@nus.edu.sg.

Received for review June 15, 2011 and accepted July 27, 2011.

Published online July 27, 2011
10.1021/nn202190c

be derived by the chemical oxidation and exfoliation of graphite. Epoxide, carboxyl, and hydroxyl groups present on the basal plane and edges of GO enable greater interactions with proteins through covalent, electrostatic, and hydrogen bonding.

Recently, the ability of CVD grown G to promote the adhesion and proliferation of MSCs and osteoblasts has been demonstrated.[17] In the presence of osteogenic chemical inducers, MSCs cultured on G substrates exhibited early maturation and mineralization.[18] Although the ability of G in modulating osteogenic differentiation is evident, the origin of how it can accelerate stem cell renewal and differentiation is not known. To investigate if this is correlated to the chemical properties of G, we investigated the effects of G and GO substrates on the adipogenic and osteogenic differentiation of MSCs. The chemical interactions between the substrates and the chemical inducers were also examined using optical spectroscopy techniques to derive molecular insights into the enhancement mechanism. Of central interest in this study is whether G and GO, through molecular binding interactions, can act as preconcentrating platforms for the soluble factors required for stem cell growth and differentiation. If so, G and GO could become ideal substrates for the effective specification of stem cell fate in the presence of multiple chemical stimuli.

RESULTS AND DISCUSSION

Characterization of Substrates. The G films employed in this study were grown by chemical vapor deposition using a reported procedure.[19] GO was synthesized using Hummers' method.[20,21] Polydimethylsiloxane (PDMS) was used as a reference material and a support for G and GO [detailed experimental procedures can be found in the Supporting Information]. Raman spectroscopy was used to verify the quality of CVD graphene film (see Supporting Information Figure S1). The negligible defect-related peak at around 1350 cm^{-1} indicates the high crystallinity of the G film. However, the oxygen functionalities on GO disrupt the extensive sp^2 conjugation, giving rise to an I_D/I_G ratio of 1.07. The chemical environments of G and GO were also analyzed by X-ray photoelectron spectroscopy (XPS), as shown in Figure S1. The symmetrical C1s peak collected from G is situated at 284.6 eV and corresponds to emission from the sp^2-hybridized carbon. On the other hand, the C1s peak of GO was found to be highly asymmetrical and shows chemically shifted components at higher binding energies of 1.2, 2.3, and 3.9 eV relative to the bulk peak, which can be assigned to the hydroxyl, ether, and carboxylic groups, respectively. A tapping mode atomic force microscopy (AFM) image of CVD G on PDMS revealed the typical wrinkled topography, while GO films on PDMS exhibited a more planar surface. The substrate elasticity of G and GO

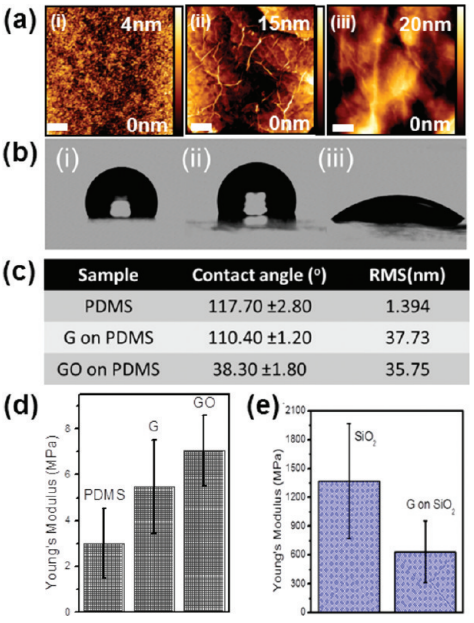

Figure 1. Surface characterization of substrates. (a) AFM topography images of (i) PDMS, (ii) G on PDMS, and (iii) GO on PDMS. (b) Contact angle images of (i) PDMS, (ii) G, and (iii) GO. (c) Table summarizing the contact angle and roughness (rms) of PDMS, G, and GO. (d) Young's modulus bar chart of PDMS, G, and GO. (e) Young's modulus bar chart of SiO_2 and G on SiO_2. Inset: white scale bar indicates 1 μm length.

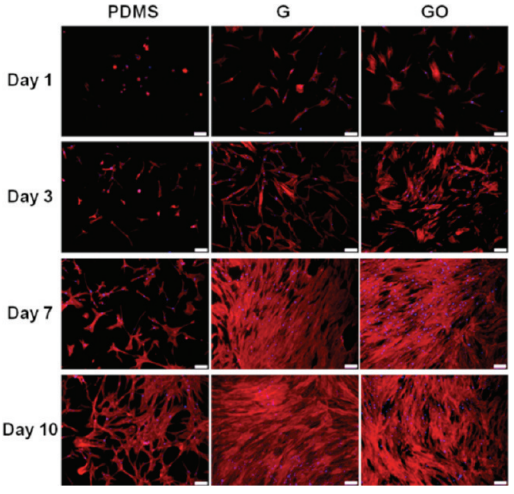

Figure 2. Fluorescent images of actin cytoskeleton of MSCs cultured on PDMS, G, and GO stained with rhodamine–phalloidin at day 1, 3, 7, and 10. Scale bars are 100 μm.

films was also measured by AFM (refer to Figure 1d). Our measurement showed that the Young's modulus values of G and GO were ~5 and 7 MPa, respectively, which were higher than that of the PDMS (~3 MPa). The apparently higher Young's modulus value of GO compared to G is due to the stacking of multiple layers of GO. In addition, G and GO have higher surface roughness (37.73 and 35.75 nm, respectively) than PDMS (1.39 nm). Contact angle measurement revealed the highly hydrophobic nature of G and PDMS, while, in contrast, GO is hydrophilic (see Figure 1b).

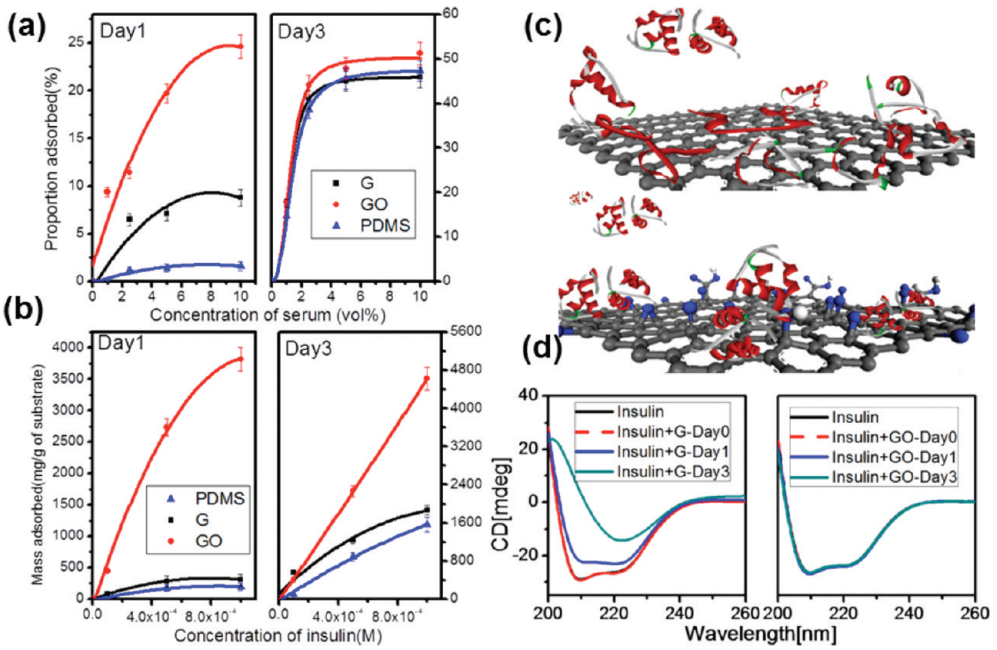

Figure 3. Loading capacity of (a) serum and (b) insulin on PDMS, G, on GO at day 1 and 3. (c) Schematic illustration of insulin adsorption on G (top panel) and GO (bottom panel). (d) Far UV absorption CD spectra of insulin in PBS with G and GO.

Cell Proliferation. In order to determine how G and GO would play a role in the cellular response and differentiation, we plated human bone marrow derived MSCs on G and GO film and used PDMS as a control substrate. Cellular morphology was evaluated by staining the F-actin fibers with phalloidin. Fluorescent images of MSCs showed that the shapes of MSCs cultured on G, GO, and PDMS were distinctively different (Figure 2). At day 1, MSCs on PDMS appeared rounder and lacked the filopodia extensions and cellular protrusions observed for cells cultured on G and GO. It can also be concluded from the number of blue-stained nuclei that there is a higher density of cells on G and GO than on the PDMS substrate. MSCs cultured on G films were homogenously dispersed on the surface and showed spindle-shape morphology, whereas those cultivated on GO films were larger and more widespread (Figure 2). However, the differences in cell morphology became less pronounced from day 7 onward.

Since serum proteins directly mediate cellular adhesion and morphology, there is a direct correlation between the adsorption capacity of the substrate for serum proteins and the subsequent cell growth. It was found that G and GO adsorbed up to 8% and 25% of the serum proteins, respectively, compared to only <1% adsorption on PDMS on day 1. It has been reported in previous studies that G and GO have remarkable loading capacities for DNA and cytochrome *c* *via* intermolecular interactions.[22] Serum is known to contain many extracellular matrix globular proteins and glycoproteins such as albumin and fibronectin.[23] Fibronectin is frequently used to coat polymeric substrates for cell culture, as it plays a major role in facilitating cell adhesion. The higher adsorption capacity of G and GO (mg/g) for serum proteins resulted in a higher density of adhesion molecules available for cell attachment and growth (Figure 3). The MSCs seeded on PDMS were round and poorly attached as compared to G and GO (Figure 2). It is known that hydrophobic substrates such as PDMS exhibit poor aqueous sample loading[24] and high resistance to protein adsorption.[25] Although G and PDMS have similar hydrophobicity, as judged from contact angle measurements (Figure 1), the π-electron cloud in G is capable of interacting with the inner hydrophobic core of proteins. Due to the presence of oxygenated groups, the hydrophilic GO can bind to serum proteins *via* electrostatic interactions.

Osteogenic Differentiation. MSCs can be induced to differentiate to osteoblasts at low density of cells of ca. 3000 cells per cm^2 in media supplemented with dexamethasone (10^{-8} M), ascorbate (0.2 mM), and β-glycerolphosphate (10 mM). After 12 days of osteogenic induction, the extent of mineralization of MSCs cultured on G, as assessed *via* Alizarin Red S staining, was found to be greater than that cultured on GO and the polydimethylsiloxane control (Figure 4). Spectrophotometric quantification confirmed these observations, with significantly higher absorbance at 450 nm (λ_{max}) for MSCs on G as compared to that on GO and PDMS ($p < 0.05$). This represents a 7-fold increase in the extent of mineralization in the MSCs cultured on G compared to the identical culture conditions for those cultured on PDMS. Using ultraviolet spectrophotometry, the loading capacities of the G, GO, and PDMS for

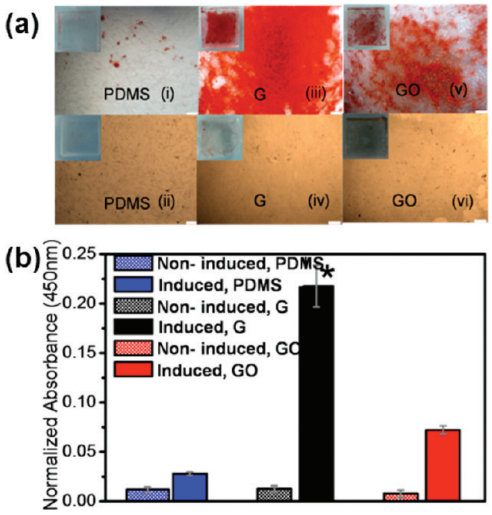

Figure 4. (a) Osteogenic differentiation visualized by Alizarin Red staining after 12 days of incubation, on PDMS (i) with induction and (ii) without induction, on G (iii) with induction and (iv) without induction, and on GO (v) with induction (vi) and without induction. Scale bars are 200 μm. (b) Quantification demonstrated a significantly higher amount of Alizarin Red staining in the MSCs differentiated on G (*$p < 0.05$; $n = 4$ for each group).

the various osteogenic chemical inducers were determined. From the adsorption isotherms obtained (Figure 5), it was found that G adsorbed the highest amount of dexamethasone (400 mg) and β-glycerolphosphate (8 g) per gram of G after 1 day of incubation.

Our experimental results indicated that MSCs cultured on G were more osteogenic and deposited more minerals under chemical induction compared to other substrates. We found that G has the ability to preconcentrate dexamethasone and β-glycerolphosphate, which are typical osteogenic inducers. The exceptionally high adsorption capacity of G for dexamethasone can be attributed to $\pi-\pi$ stacking between the aromatic rings in the biomolecules and the G basal plane. Dexamethasone is a synthetic glucocorticoid that is known to alter the expression levels of many proteins and enzymes required during bone differentiation.[26−28] Elevated levels of dexamethasone have been found to increase mineral deposition.[29] Therefore, the enhanced osteogenic differentiation of MSCs on G can be attributed to the increased local concentration of adsorbed dexamethasone. This echoes a previous study showing that the extent of osteogenic differentiation is enhanced with increasing concentration of dexamethasone in solution, with a saturation limit of 1000 nM, beyond which cell layers start to delaminate.[29] It is also worth noting that dexamethasone is not the sole chemical that is responsible for directing MSCs to osteogenic lineages. It has to act synergistically with β-glycerolphosphate along with intracellular alkaline phosphatase enzyme to synthesize new mineralized bone matrices. From the adsorption isotherms of β-glycerolphosphate obtained, G also has the highest loading capacity followed by PDMS and GO. GO, which possesses a high density of oxygen functionalities, will experience larger electrostatic repulsion from the phosphate ions compared to G and PDMS. On the other hand, the differential adsorption of ascorbic acid on these platforms (Figure 5d) can be rationalized by the degree of hydrogen bonding that is formed between the −OH moieties of the acid and the substrates. Since G has no available groups to participate in H-bonding, it adsorbs the least amount of ascorbic acid compared to GO and PDMS. PDMS has more polar groups than GO and shows a greater degree of H-binding with ascorbic acid. Although the adsorption of ascorbic acid on G is not as high compared to GO and PDMS, it has been reported that ascorbic acid was found to affect mainly postdifferentiated, mature osteoblasts.[30]

It is noteworthy that G affords accelerated differentiation of MSCs toward osteogenic differentiation. Typically, chemically induced osteogenic differentiation on polystyrene tissue culture dishes takes 21 days to complete.[4] In this case, by day 12, the MSCs on G already exhibited extensive mineralization, which points to the unique capability of G to act as a preconcentrating platform for accelerated bone differentiation. Besides considering the chemical interactions between the substrates and soluble factors involved in osteogenic specification, we consider whether the mechanical properties of the substrates have a significant role in influencing the fate of the stem cell. It has been reported by Engler *et al*. that stiff substrates (>100 kPa) promote bone differentiation.[2] However, since the elasticity of G, GO, and PDMS (1:10) were found to be in the same order of magnitude (∼3−7 MPa), this suggests that the differences in cell differentiation were unlikely to be due to substrate stiffness. In addition, due to the thinness of G, the substrate supporting G has a dominant influence of the overall stiffness. For example, the elastic modulus of G measured on silicon is approximately 600 MPa, which is 2 orders higher than on PDMS (refer to Figure 1e). Therefore, stiffness is not a differentiating factor in this case since the stiffness is dominated by the substrate supporting G.

It is well established that when stem cells are subjected to physical stresses exerted by topographic features on the substrate, stem cell differentiation into specific cell lineages can be enhanced.[2,31−33] Dalby *et al*.[3] reported that MSCs cultured on randomized poly(methylmethacrylate) nanopatterns exhibited MSC osteoblastic morphologies after 21 days of incubation in standard cell culture media in the absence of chemical inducers. Although we cannot rule out the possibility that the corrugated structure of G, arising from its surface ripples and folds, can have some role in mediating osteogenesis, the fact that extensive mineralization was observed only on MSCs cultured in osteogenic induction media suggests that the chemical binding

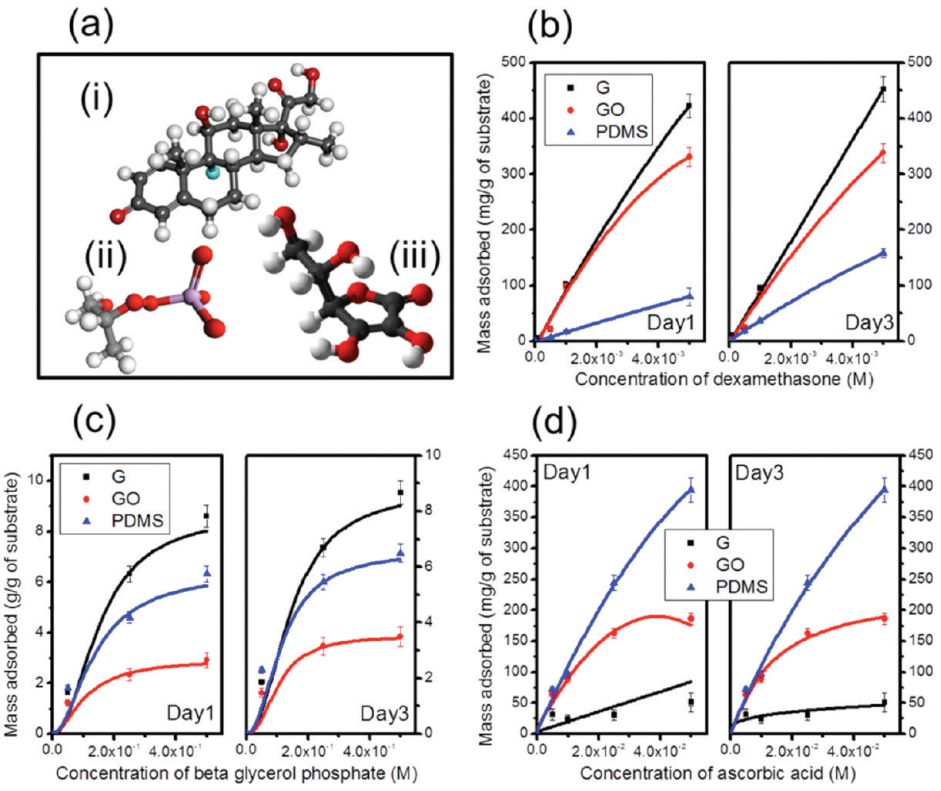

Figure 5. (a) Three-dimensional chemical structure of (i) dexamethasone, (ii) beta glycerol phosphate anion, and (iii) ascorbic acid and loading capacity of (i), (ii), and (iii) in (b), (c), and (d), respectively, in osteogenic induction media on PDMS, G, and GO.

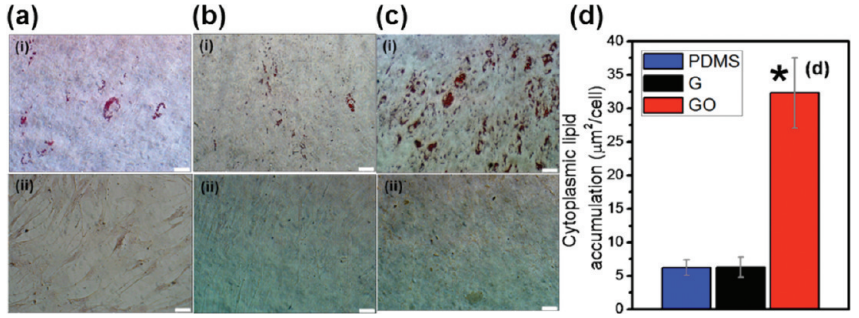

Figure 6. Extent of cytoplasmic lipid accumulation assessed by Oil Red O staining after 14 days of induction on (a) PDMS (i) with induction and (ii) without induction, on (b) G (i) with induction and (ii) without induction, and on (c) GO (i) with induction and (ii) without induction. Scale bars are 50 μm. (d) A higher propensity for adipogenic differentiation was observed for the MSCs differentiated on GO, with a significantly larger amount of fat accumulation than the MSCs differentiated on G (b(i)) and PDMS (a(i)) (*$p < 0.05$; $n = 4$ for each group). In negative controls without any adipogenic induction chemicals, no lipid deposits were observed.

effect of G toward the growth agent is the key in accelerating MSC bone differentiation.

Adipogenic Differentiation. Adipogenic differentiation is usually observed at a high density of ca. 20 000 cells per cm^2 with supplements of dexamethasone (10^{-6} M), indomethacin (0.6×10^{-4} M), and insulin (4 μg/mL). The adipogenic differentiation rate of MSCs was determined by specifically staining intracytoplasmic lipids with Oil Red O[34] and its amount quantified *in situ* (see Methods). Figure 6 shows adipogenic differentiation of MSCs cultured on the different substrates investigated in this study. Interestingly, the situation is reversed when MSCs were chemically induced to differentiate into adipocytes on G and GO. The results indicated that G suppressed adipogenesis with 6.29 μm^2/cell of lipid accumulation, while GO strongly enhanced adipogenesis with 32.3 μm^2/cell relative to MSCs differentiated on PDMS. It was noted that no lipid globules were detected on all three control, non-induced substrates. As insulin is the main mediator for fatty acid synthesis,[35] we measured the adsorption isotherms of insulin on G and GO. Figure 3 shows that GO exhibited the highest adsorption capacity of ca. 4800 mg of insulin per gram of GO as compared to

1900 mg of insulin per gram of G and 1580 mg of insulin per gram of PDMS.

Since any alteration to the configuration of adsorbed insulin might interfere with its function to regulate fatty acid synthesis, the 3D conformation of the adsorbed insulin was investigated *via* circular dichroism (CD). Our measurements revealed that the immobilized insulin on G was denatured, which can be judged from the attenuated negative absorption peaks at 209.0 and 222.0 nm corresponding to the α-helix and β-pleated sheets, respectively at day 1 and 3 (see Figure 3d). To ascertain that any discrepancy observed in the absorption profile is not due to self-aggregation of insulin, its high tension voltage curves were recorded (Figure S2). Upon incubation with G for one day, the peak representative of α-helix diminished by 13.4% and is unobservable by day 3, while the β-pleated sheets peak was found to decrease merely by 17.0%. From these data obtained, it can be concluded that denaturation of insulin occurs due to the unravelling of its α-helix domains, while the effect on the β-pleated sheet component was less pronounced.

Adipogenesis is enhanced on GO due to its high affinity for insulin, which is the main mediator for fatty acid synthesis. The ability of GO to undergo H-bonding and electrostatic interactions enhances its binding capacity for insulin by more than twice compared to G on day 3. This explains the occurrence of higher lipid accumulation for the MSCs differentiated on GO. Despite the higher affinity of GO for insulin, the electrostatic binding interaction with the protein allows the latter to maintain its three-dimensional conformation, thereby enhancing adipogenic differentiation on GO. Since no fat globules were observed on the non-induced GO substrate, it is unlikely that adipogenesis is mediated by the substrate nanotopography alone. Although the adsorption of insulin on G is higher than on PDMS, less fat globules were observed (Figure 6). This can be attributed to the denaturation of insulin brought about by strong $\pi-\pi$ stacking on G. Our CD measurements revealed that the immobilized insulin on G was denatured, which is evident from changes in the negative absorption peaks of the α-helix at 209.0 nm and β-pleated sheets at 222.0 nm. Essentially, the different chemical structure of G and GO differentiates their binding interactions with biomolecules in terms of immobilization with or without denaturation.

CONCLUSIONS

This study elucidates the origin of accelerated mesenchymal stem cell adhesion, proliferation, and differentiation on G and GO substrates. The origin of the osteogenic differentiation is traced to the ability of G to act as a preconcentration platform for osteogenic inducers, namely, dexamethasone and β-glycerolphosphate. We also demonstrate that insulin, which is a main mediator for fatty acid synthesis, is denatured upon adsorption on G through strong $\pi-\pi$ interaction and unravelling of its three-dimensional configuration. Conversely, insulin is not denatured on GO, and its high affinity for insulin greatly enhances adipogenic differentiation. Therefore, besides the specific binding interactions, the denaturation, or not, of the inducers is an important factor in determining the fate of the stem cell. In summary, G and GO are demonstrated to be effective preconcentration platforms for accelerated stem cell growth and differentiation through molecular interactions. It is highly possible that interactions with various chemical inducers could facilitate stem cell differentiation toward other lineages. The ability of G and GO to accelerate stem cell differentiation should find diverse applications in tissue engineering and regenerative medicine.

METHODS

G and GO Film Preparation. The transfer technique employed in this study to transfer the G or GO films to PDMS (Dow Corning) is similar to previously reported methods.[36] GO film was prepared through the use of a Langmuir–Blodgett (LB) trough (Nima Technologies). GO was dispersed in water–methanol (1:5) solution at a concentration of 1 mg/mL. The surface of the water-filled LB trough was cleaned several times by aspiration. Then 100 μL of the GO solution was deposited on the water-filled LB trough. After 30 min of equilibration, the film was compressed to a surface pressure value of 20 mN/m. The GO film was formed by dip-coating the PDMS substrate several times.

Characterization. Raman spectra of G and GO film were obtained with a WITEC CRM200 Raman spectrometer at room temperature, with an excitation laser source of 532 nm. The laser power was kept below 0.1 mW to prevent heating of the sample. The hydrophilicity of the samples was investigated using contact angle measurements (VCA Optima, AST Products Inc.). XPS was performed using an unmonochromated Al Kα X-ray source at 1486.6 eV (Thermo VG Scientific, UK) with a Phobios 100 electron analyzer (SPECS GmbH, Germany) equipped with 5 channeltrons. The pass energy of the analyzer was fixed at 50 eV for wide scan and 20 eV for narrow scan, and the takeoff angle was normal to the sample.

Spectrophotometry for Determination of Loading Capacities. Dexamethasone, β-glycerolphosphate, ascorbic acid, and insulin (obtained from Sigma-Aldrich and used without further purification) with concentrations ranging from 10^{-4} to 10^{-1} M were prepared in phosphate buffer. Fetal bovine serum (Gibco) was reconstituted in DMEM at 1, 2, 5, and 10% (v/v) for spectrophotometric measurement. PDMS, G, and GO (1 mg/mL) in PBS were sonicated for 1 h prior to usage, to ensure the formation of a homogeneous dispersion. The chemical agents (0.5 mL) were mixed with PDMS, G, or GO (0.5 mL) and vortexed in a shaker for equilibration. After which, the mixture was centrifuged (14 000 rpm, 10 min), the supernatant was collected, and spectrophotometric measurements were conducted on day 1 and 3. The adsorption isotherm of the respective chemical agent was obtained using UV–vis

spectroscopy. The amount of chemical agent adsorbed was determined from the change in protein adsorption before and after the addition of PDMS, G, and GO using a UV−vis spectrophotometer (NanoDrop 2000, Thermo Scientific).

Circular Dichroism Spectroscopy. Each CD spectrum and its corresponding high tension voltage curve were recorded on a Jasco J-810 spectropolarimeter using a quartz cell with an optical path length of 1 mm. The scanning speed was set at 50 nm/min, and the wavelength range was set at 190−260 nm. All samples were prepared in phosphate-buffered saline (PBS) adjusted to ~pH 7.4. By considering the specific areas of G and GO to be 2630 m^2/g,[20,37] 0.3125 mg/mL of insulin and 0.025 mg/mL of G and GO were used to simulate the conditions of the cell culture environment. All spectra collected were obtained from an average of three consecutive scans.

Cell Culture. Human bone marrow derived MSCs were obtained from commercial sources (Lonza). Cells were cultured in a humidity-controlled environment under 5% CO_2 and fed every 3 days with Dulbecco's modified Eagle's medium (Gibco), supplemented with 10% fetal bovine serum (Invitrogen) and 1% penicillin/streptomycin (Invitrogen). Cells were received at passage 1, expanded at ~5000 cells/cm^2, and subcultured at 70−80% confluence. Passage 4 cells were used in the experiments. MSCs were applied at 1000 cells per cm^2 for time course study of cell morphology. Cells were fixed in 4% paraformaldehyde (Sigma-Aldrich), stained with rhodamin phalloidin (Invitrogen), costained with 4′,6-diamidino-2-phenylindole (DAPI) (Sigma-Aldrich), and imaged under an epi-fluorescence microscope (Olympus IX81, Olympus Inc.) at day 1, 4, 7, and 10.

Osteogenic Differentiation. MSCs were seeded at 2500 cells/cm^2 and cultured for two weeks in DMEM with 10% FBS, 10 mM β-glycerophosphate (Sigma-Aldrich), 10^{-8} M dexamethasone (Sigma-Aldrich), and 0.2 mM ascorbate (Sigma-Aldrich) and with medium changes every 3 days. Noninduced control MSCs were fed only basal medium with 10% FBS and 1% penicillin/streptomycin on the same schedule. After 12 days of induction, cells were stained with Alizarin Red (Sigma-Aldrich) and extracted with 20% methanol and 10% acetic acid for spectrophotometric quantification at 450 nm using a Nanodrop UV−vis spectrophotometer (Thermo Scientific).

Adipogenic Differentiation. MSCs were plated at 2×10^4 cells/cm^2 and induced to differentiate for 14 days in DMEM with 10% FBS, 10^{-6} M dexamethasone (Sigma-Aldrich), 5 μg/mL insulin (Sigma-Aldrich), and 0.6×10^{-4} M indomethacin (Sigma-Aldrich). Non-induced control MSCs were fed only basal medium with 10% FBS and 1% penicillin/streptomycin on the same schedule. After 14 days of induction, cells were rinsed with PBS, fixed in 4% methanol-free formaldehyde (Sigma-Aldrich), then stained with Oil Red O (Sigma-Aldrich), and costained with DAPI for 30 min. The stained cells were observed under an epi-fluorescence microscope (Olympus IX81, Olympus Inc.). Quantification of adipogenic differentiation by MetaMorph 6.3v3 was based on measuring the total number of Oil Red O red pixels, then normalizing to nuclei count based on detected DAPI fluorescence. The end data correspond to the total area of lipid droplets present per cell (μm^2). The area measurements were imported into Microsoft Excel, and the mean ± SD of the areas was calculated.

AFM Imaging and Indentation. All data were acquired in PBS at room temperature on a NanoWizard II AFM (JPK Instruments) coupled with an inverted microscope (Olympus). For images captured in contact mode, HYDRA2R-100NG probes (Applied NanoStructures) were used. HSC 20 probes with a defined hemispherical tip shape of ~20 nm in radius (~0.4 N/m) (Nanoscience Instruments) were used for indentation experiments. Indentation was carried out at the clean spots immediately after scanning the same area using the same probe. The ramp size in this study was 1 μm, and the loading speed was 1 μm/s. An indentation force of 3 to 30 nN was applied during the tests in order to ensure that the indentation depth is less than 20 nm. The Young's modulus was subsequently determined using Hertz's contact model using JPK Data Processing software (JPK Instruments).

Statistical Analysis. The statistical differences were analyzed ($n = 4$) by a paired Student's t test; p values less than 0.05 were considered to indicate statistical differences (95% confidence interval).

Acknowledgment. K.P.L. thanks NRF-CRP for the grant Graphene Related Materials and Devices (R-143-000-360-281).

Supporting Information Available: Detailed experimental procedures and additional figures. This material is available free of charge via the Internet at http://pubs.acs.org.

REFERENCES AND NOTES

1. Meirelles, L.; Chagastelles, P. C.; Nardi, N. B. Mesenchymal Stem Cells Reside in Virtually All Post-Natal Organs and Tissues. *J. Cell Sci.* **2006**, *119*, 2204–2213.
2. Engler, A. J.; Sen, S.; Sweeney, H. L.; Discher, D. E. Matrix Elasticity Directs Stem Cell Lineage Specification. *Cell* **2006**, *126*, 677–689.
3. Dalby, M. J.; Gadegaard, N.; Tare, R.; Andar, A.; Riehle, M. O.; Herzyk, P.; Wilkinson, C. D. W.; Oreffo, R. O. C. The Control of Human Mesenchymal Cell Differentiation Using Nanoscale Symmetry and Disorder. *Nat. Mater.* **2007**, *6*, 997–1003.
4. Pittenger, M. F.; Mackay, A. M.; Beck, S. C.; Jaiswal, R. K.; Douglas, R.; Mosca, J. D.; Moorman, M. A.; Simonetti, D. W.; Craig, S.; Marshak, D. R. Multilineage Potential of Adult Human Mesenchymal Stem Cells. *Science* **1999**, *284*, 143–147.
5. Treiser, M. D.; Yang, E. H.; Gordonov, S.; Cohen, D. M.; Androulakis, I. P.; Kohn, J.; Chen, C. S.; Moghe, P. V. Cytoskeleton-Based Forecasting of Stem Cell Lineage Fates. *Proc. Natl. Acad. Sci. U. S. A.* **2010**, *107*, 610–615.
6. Jung, D. R.; Kapur, R.; Adams, T.; Giuliano, K. A.; Mrksich, M.; Criaghead, H. G.; Taylor, D. L. Topographical and Physicochemical Modification of Material Surface to Enable Patterning of Living Cells. *Crit. Rev. Biotechnol.* **2001**, *21*, 111–154.
7. Mahdavi, A.; Ferreira, L.; Sundback, C.; Nichol, J. W.; Chan, E. P.; Carter, D. J. D.; Bettinger, C. J.; Patanavanich, S.; Chignozha, L.; Ben-Joseph, E.; *et al.* A Biodegradable and Biocompatible Gecko-Inspired Tissue Adhesive. *Proc. Natl. Acad. Sci. U. S. A.* **2008**, *105*, 2307–2312.
8. Li, W. J.; Tuli, R.; Huang, X.; Laquerriere, P.; Tuan, R. S. Multilineage Differentiation of Human Mesenchymal Stem Cells in a Three-Dimensional Nanofibrous Scaffold. *Biomaterials* **2005**, *26*, 5158–5166.
9. Marletta, G.; Ciapetti, G.; Satriano, C.; Perut, F.; Salerno, M.; Baldini, N. Improved Osteogenic Differentiation of Human Marrow Stromal Cells Cultured on Ion-induced Chemically Structured Poly-ε-caprolactone. *Biomaterials* **2007**, *28*, 1132–1140.
10. Prabhakaran, M. P.; Venugopal, J. R.; Ramakrishna, S. Mesenchymal Stem Cell Differentiation to Neuronal Cells on Electrospun Nanofibrous Substrates for Nerve Tissue Engineering. *Biomaterials* **2009**, *30*, 4996–5003.
11. Xin, X.; Hussain, M.; Mao, J. J. Continuing Differentiation of Human Mesenchymal Stem Cells and Induced Chondrogenic and Osteogenic Lineages in Electrospun PLGA Nanofiber Scaffold. *Biomaterials* **2007**, *28*, 316–325.
12. Mooney, E.; Dockery, P.; Greiser, U.; Murphy, M.; Barron, V. Carbon Nanotubes and Mesenchymal Stem Cells: Biocompatibility, Proliferation and Differentiation. *Nano Lett.* **2008**, *8*, 2137–2143.
13. Yi, C.; Liu, D.; Fong, C. C.; Zhang, J.; Yang, M. Gold Nanoparticles Promote Osteogenic Differentiation of Mesenchymal Stem Cells through p38 MAPK Pathway. *ACS Nano* **2010**, *4*, 6439–6448.
14. Kaur, G.; Valarmathi, M. T.; Potts, J. D.; Jabbari, E.; Sabo-Attwood, T.; Wang, Q. Regulation of Osteogenic Differentiation of Rat Bone Marrow Stromal Cells on 2D Nanorod Substrates. *Biomaterials* **2010**, *31*, 1732–1741.
15. Kaur, G.; Valarmathi, M. T.; Potts, J. D.; Wang, Q. The Promotion of Osteoblastic Differentiation of Rat Bone Marrow Stromal Cells by a Polyvalent Plant Mosaic Virus. *Biomaterials* **2008**, *29*, 4074–4081.
16. Bae, S.; Kim, H.; Lee, Y.; Xu, X.; Park, J. S.; Zheng, Y.; Balakrishnan, J.; Lei, T.; Ri Kim, H.; Song, Y. I.; *et al.* Roll-to-Roll Production of 30-in. Graphene Films for Transparent Electrodes. *Nat. Nanotechnol.* **2010**, *5*, 574–578.

17. Kalbacova, M.; Broz, A.; Kong, J.; Kalbac, M. Graphene Substrates Promote Adherence of Human Osteoblasts and Mesenchymal Stromal Cells. *Carbon* **2010**, *48*, 4323–4329.
18. Nayak, T. R.; Andersen, H.; Makam, V. S.; Khaw, C.; Bae, S.; Xu, X.; Ee, P. R.; Ahn, J. H.; Hong, B. H.; Pastorin, G.; *et al*. Graphene for Controlled and Accelerated Osteogenic Differentiation of Human Mesenchymal Stem Cells. *ACS Nano* **2011**, *5*, 4670–4678.
19. Li, X.; Cai, W.; An, J.; Kim, S.; Nah, J.; Yang, D.; Piner, R.; Velamakanni, A.; Jung, I.; Tutuc, E.; *et al*. Large-Area Synthesis of High-Quality and Uniform Graphene Films on Copper Foils. *Science* **2009**, *324*, 1312–1314.
20. Hummers, W. S., Jr.; Offeman, R. E. Preparation of Graphitic Oxide. *J. Am. Chem. Soc.* **1958**, *80*, 1339.
21. Stankovich, S.; Dikin, D. A.; Piner, R. D.; Kohlhaas, K. A.; Kleinhammes, A.; Jia, Y.; Wu, Y.; Nguyen, S. T.; Ruoff, R. S. Synthesis of Graphene-Based Nanosheets Via Chemical Reduction of Exfoliated Graphite Oxide. *Carbon* **2007**, *45*, 1558–1565.
22. Tang, L. A. L.; Wang, J.; Loh, K. P. Graphene-Based SELDI Probe with Ultrahigh Extraction and Sensitivity for DNA Oligomer. *J. Am. Chem. Soc.* **2010**, *132*, 10976–10977.
23. Oh, S.; Brammer, K. S.; Li, Y. S. J.; Teng, D.; Engler, A. J.; Chien, S.; Jin, S. Stem Cell Fate Dictated Solely by Altered Nanotube Dimension. *Proc. Natl. Acad. Sci. U. S. A.* **2009**, *106*, 2130–2135.
24. Phillips, K. S.; Cheng, Q. Assembly and Characterization of Protein Resistant Planar Bilayers in PDMS Microfluidic Devices. *Mater. Res. Soc. Symp. Proc.* **2003**, 774:O7.2.1–O7.2.8.
25. Sapsford, K. E.; Ligler, F. S. Real-time Analysis of Protein Adsorption to a Variety of Thin Films. *Biosens. Bioelectron.* **2004**, *19*, 1045–1055.
26. Haynesworth, S. E.; Goshima, J.; Goldberg, V. M.; Caplan, A. I. Characterization of Cells with Osteogenic Potential from Human Marrow. *Bone* **1992**, *13*, 81–88.
27. Oshina, H.; Sotome, S.; Yoshii, T.; Torigoe, I.; Sugata, Y.; Maehara, H.; Marukawa, E.; Omura, K.; Shinomiya, K. Effects of Continuous Dexamethasone Treatment on Differentiation Capabilities of Bone Marrow-Derived Mesenchymal Cells. *Bone* **2007**, *41*, 575–583.
28. Scutt, A.; Bertram, P.; Bräutigam, M. The Role of Glucocorticoids and Prostaglandin E2 in the Recruitment of Bone Marrow Mesenchymal Cells to the Osteoblastic Lineage: Positive and Negative Effects. *Calcif. Tissue Int.* **1996**, *59*, 154–162.
29. Jaiswal, N.; Haynesworth, S. E.; Caplan, A. I.; Bruder, S. P. Osteogenic Differentiation of Purified, Culture-Expanded Human Mesenchymal Stem Cells in Vitro. *J. Cell. Biochem.* **1997**, *64*, 295–312.
30. Quarles, L. D.; Yohay, D. A.; Lever, L. W.; Caton, R.; Wenstrup, R. J. Distinct Proliferative and Differentiated Stages of Murine MC3T3-El Cells in Culture: An in Vitro Model of Osteoblast Development. *J. Bone Miner. Res.* **1992**, *7*, 683–692.
31. Altman, G. H.; Horan, R. L.; Martin, I.; Farhadi, J.; Stark, P. R.; Volloch, V.; Richmond, J. C.; Vunjak-Novakovic, G.; Kaplan, D. L. Cell Differentiation by Mechanical Stress. *FASEB J.* **2002**, *16*, 270–272.
32. Dalby, M. J.; McCloy, D.; Robertson, M.; Agheli, H.; Sutherland, D.; Affrossman, S.; Oreffo, R. O. C. Osteoprogenitor Response to Semi-ordered and Random Nanotopographies. *Biomaterials* **2006**, *27*, 2980–2987.
33. Yamamoto, K.; Sokabe, T.; Watabe, T.; Miyazono, K.; Yamashita, J. K.; Obi, S.; Ohura, N.; Matsushita, A.; Kamiya, A.; Ando, J. Fluid Shear Stress Induces Differentiation of Flk-1-Positive Embryonic Stem Cells into Vascular Endothelial Cells in Vitro. *Am. J. Physiol.* **2005**, *288*, H1915–H1924.
34. Liu, D.; Yi, C.; Zhang, D.; Zhang, J.; Yang, M. Inhibition of Proliferation and Differentiation of Mesenchymal Stem Cells by Carboxylated Carbon Nanotubes. *ACS Nano* **2010**, *4*, 2185–2195.
35. Hauner, H.; Schmid, P.; Pfeiffer, E. F. Glucocorticoids and Insulin Promote the Differentiation of Human Adipocyte Precursor Cells into Fat Cells. *J. Clin. Endocrinol. Metab.* **1987**, *64*, 832–835.
36. Wang, Y.; Tong, S. W.; Xu, X. F.; Özyilmaz, B.; Loh, K. P. Interface Engineering of Layer-by-Layer Stacked Graphene Anodes for High-Performance Organic Solar Cells. *Adv. Mater.* **2011**, *23*, 1514–1518.
37. Liu, Z.; Robinson, J. T.; Sun, X.; Dai, H. PEGylated Nanographene Oxide for Delivery of Water-Insoluble Cancer Drugs. *J. Am. Chem. Soc.* **2008**, *130*, 10876–10877.